

ULRR

Analysis of sintered wicked heat pipes for space constrained multiple component cooling

Item Type	Article
Authors	Mooney, Joseph Phelim;Egan, Vanessa;Quinlan, Ruairi;Punch, Jeff
Citation	IEEE Transactions on Components, Packaging and Manufacturing Technology;11 (11), pp. 1896-1908
Publisher	IEEE Computer Society
Download date	2026-04-20 16:38:59
Item License	https://creativecommons.org/licenses/by-nc-sa/1.0/
Link to Item	https://hdl.handle.net/10344/10828

Analysis of Sintered Wicked Heat Pipes for Space Constrained Multiple Component Cooling

Joseph P Mooney^{a,b,*}, Vanessa Egan^{a,b}, Ruairi Quinlan^b, Jeff Punch^{a,b}

* Corresponding Author

^aCONNECT, Stokes Laboratories, Bernal Institute, University of Limerick, V94 T9PX, Ireland

^bSchool of Engineering, University of Limerick, V94 T9PX, Ireland

V94 T9PX

Email: Joseph.mooney@ul.ie

Abstract - Contemporary electronic cooling applications can feature complex heat pipe configurations with multiple heat sources (MHS), and one or more bends in various locations to meet physical constraints. It is typically understood that implementing a bend or adding MHS to a heat pipe that was tested for a straight single heat source (SHS) heat pipe can degrade thermal performance. However, the severity of combining the two phenomenon and the effects of changing the location of a bend in a MHS heat pipe are unknown. In this context, this study presents an experimental investigation of the thermal performance of four configurations for 400 mm long, 6 mm diameter; cylindrical copper sintered heat pipes, where small, heated copper saddles are configured as evaporators: a pipe with a SHS; a pipe with MHS; an MHS heat pipe with an increasing bend angle from 0° – 90°; and an MHS heat pipe where the location of a 90° bend is moved along the axis. The results demonstrate that a bent MHS heat pipe does not act in a similar manner to a conventional SHS heat pipe or a straight MHS heat pipe. It was found that the thermal resistance increases by up to 65% when the configuration is changed from SHS to MHS, and bend angle is found to increase the resistance by a further 15-65%. For the MHS cases, bend location induces resistance increases of ~5-18%. Furthermore, the optimum bend location for the MHS case is found to be adjacent to the middle evaporator (of five), for cases in which the heat load is evenly distributed before and after the bend. The results suggest that the combination of MHS, bend angle and bend location have unique effects on the fluid transport mechanisms inside the heat pipe and, thus, thermal performance changes between bend location configurations. Therefore, it is concluded that a bent MHS heat pipe configuration should not be designed on the basis of the thermal characteristics for straight SHS heat pipes.

KEYWORDS

Heat pipe, multiple heat sources, effective thermal conductivity, bending, electronics cooling.

NOMENCLATURE

Roman Letters

A	Area, m ²
d	Diameter, mm
I	Current, A
k	Thermal conductivity, W/m . K
L	Length, mm
P _w	Power, W
Q	Heat, W
r	Radius, mm
R _{th}	Thermal resistance, K/W
T	Temperature, °C
V	Voltage, V
x	distance, mm

Greek Symbols

θ	Angle, °
ρ	Density, kg/m ³
σ	Surface Tension, N/m

Subscripts

c	Condenser
e	Evaporator
eff	Effective
i	Inner
l	Liquid
l-v	Liquid-vapor
o	Outer
max	Maximum
s	Saddle
v	Vapor

Dimensionless Numbers

We	Weber Number
----	--------------

Abbreviations

G	Generation
MHS	Multi Heat Source
NCG	Non-Condensable Gas
PA	Power Amplifier
PCB	Printed Circuit Board
SHS	Single Heat Source

I. INTRODUCTION

Two-phase heat transfer devices have become increasingly important for the thermal management of electronic components. Reported investigations of heat pipes for thermal management applications have generally addressed single heat source (SHS) configurations [1-4], using a range of performance characteristics (e.g., total thermal resistance and effective thermal conductivity). There is an abundance of both numerical and experimental literature on topics relating to the SHS configuration [1-3]. Recently, however, as a result of steady increases in power and decreases in the volume of electronics assemblies, heat dissipation has become an increasingly critical problem [5]. Over many years heat pipes have developed and diversified to satisfy these stringent requirements. Currently there is a range of heat pipe types, such as flat heat pipes [6, 7], loop heat pipes [8], thermosyphons [9], pulsating heat pipes [10] and micro heat pipes [11], amongst others. Moreover, the design of the passive wicking structures has progressed to reduce the likelihood of ‘dry-out’ occurring in a heat pipe. Dry-out is described by the lack of fluid available, or the “drying out” of the wick in the heat pipe’s evaporator section, due

to excessive heat fluxes or insufficient design of the heat pipe's capillary structure [1].

The selection of a heat pipe for an application depends on many factors, such as cost, size, ease of implementation and maintenance, and the thermal requirement. A commonly-used heat pipe for electronics cooling applications is a sintered copper water heat pipe. This heat pipe is known as a homogeneous wicked heat pipe because the wick comprises a single material with an axially-invariant cross sectional structure [12]. Applications range from laptop and smart phone cooling to the thermal management of batteries for electric vehicles [13]. This type of heat pipe is used for its ease of implementation, low manufacture cost, high performance and malleability.

With the continuous improvements in miniaturization and integration, electronic devices now contain an increasing number of heat sources. For example, a wireless basestation could feature multiple CPUs [14, 15] and multiple high-power chips (such as power-amplifiers) packaged on the same printed circuit board (PCB). For these multi-heat source systems, a heat dissipation scheme comprising multiple heat pipes is conventionally adopted. For example, *McGlen et al.* [16] utilized three heat pipes to maintain the temperature of three heat dissipating chips below 70 °C. Although this method was effective and simple, it requires a large volume and low spatial utilization [17]. An alternative approach would be to implement a larger heat pipe and use it to cool multiple components in the circuit, a configuration known as multi-heat source (MHS) heat pipes. The number of evaporators required to be cooled by a single heat pipe can influence the thermal performance of the pipe. Recently, efforts have been employed to analyze the performance of a heat pipe when it is subject to multiple heat sources. Figure 1 illustrates this phenomenon and how it can impact the working fluid inside a heat pipe.

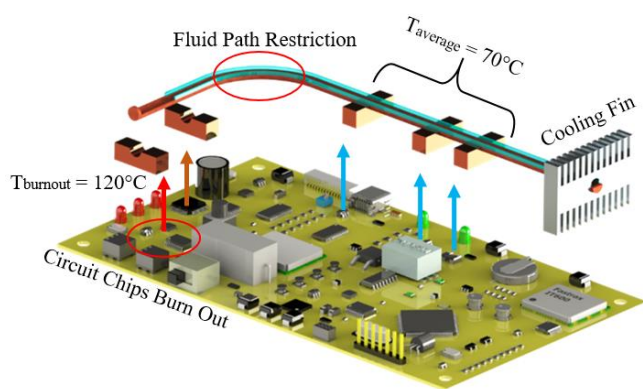


Figure 1: An MHS heat pipe configuration, illustrating the potential phenomenon of heat pipe dry-out.

A significant problem that affects the performance of a heat pipe can arise when the evaporator configuration is changed from SHS to MHS. This problem was addressed by *Boo et al.* [18] when they compared SHS configuration to MHS configuration with five, equal and unequal loaded, evaporators. At higher thermal loads (300 W), the thermal resistance of the heat pipe increased by up to 40% as it was changed from SHS to MHS with equal loads. The largest increase in thermal resistance, however, was observed at lower thermal loads, of ~50 W. Where an increase of up to 90% was observed, 0.16 K/W to ~0.32 K/W. The addition

of extra variables to the heat pipe, such as unequal MHS loads, increased the overall thermal resistance by almost a factor of two.

On another note, multiple sources can be separated by uniform or non-uniform distances, where the thermal performance of a heat pipe can change depending on the distance between the heat sources and how far they are from the condenser. *Tharawadee et al.* [19] presented a numerical analysis on this by utilizing two heat sources cooled by one condenser, and showed that moving two heat sources further apart, from 0 mm to 75 mm, induced a small decrease in thermal resistance, from 0.59 K/W to 0.53 K/W.

To date, studies on MHS configurations have mainly focused on sources arranged in either a column or row [18, 19]. These studies are somewhat incomplete representations of practical applications in electronics cooling. For space constrained applications, straight heat pipes are conventionally bent in between each heat dissipating component (i.e., groups of evaporators) to navigate around other heat sensitive components, as seen in figure 1. The implementation of a deformity (i.e., a bend) can influence the thermal behavior of a heat pipe. A recent experimental study [4] on a 6 mm heat pipe investigated the effect of bending and flattening on the thermal resistance. As the bend angle was varied from 0° to 90°, the thermal resistance increased by 21.5%. It was speculated that this increase in resistance was caused by the deformation of the wick, which primarily obstructed the liquid phase flow. Two types of wick deformation were assumed to occur due to bending: 1. particles separated from one another at the outer radius of the bend, creating larger pores for the liquid return flow; and 2. particles buckled together at the pipe's inner radius at the bend, closing portions of the capillary structure for liquid return flow.

Further analysis on bent heat pipes found that the deformation can have a severe effect on the maximum allowable heat input before the onset of dry-out. *Jiang et al.* [20] found that as bend angle increased from 0° to 45° and 90°, the maximum heat input reduced from 50 W to 35 W and 30 W before dry-out occurred. Similarly, the thermal resistance rose by ~30% from 0.07 K/W to 0.09 K/W at a 25 W heat input. This study speculated that the increase in thermal resistance due to bending was solely caused by the obstruction in the flow of liquid returning to the evaporator from the condenser.

It is evident from the experimentation reported in the literature [4, 19, 21, 22] that the performance of a heat pipe is significantly reduced when changing from SHS to MHS configuration, and also when bending the pipe from 0°–90°. The combination of these phenomena has not been previously investigated in the literature, however. Moreover, a relationship between the location of a bend and the thermal performance of an MHS heat pipe has not been studied. Hence, to gain a deeper insight into the common practical deployments of heat pipes, the current study presents an experimental investigation into the combined effects of bending and changing the location of the bend in an MHS heat pipe, where straight SHS and MHS configurations are used as base cases. Results demonstrate that the performance of an MHS heat pipe is significantly degraded when it is bent, and that the thermal performance of the bent MHS heat pipe is a function of bend location and heat input. Experimental data suggest that an optimum bend location exists in a MHS configuration, and that this resides between the MHSs.

II. EXPERIMENTAL SETUP

This section presents the experimental apparatus and set up to test the thermal performance of a sintered copper heat pipe in multiple configurations that aim to resemble a complex cooling solution. In total, eight MHS configurations were tested and compared to a base SHS configuration. The apparatus was initially used to verify that the thermal performance of the heat pipe was reduced when changing from SHS to MHS, as per the literature [18]. Then, the effects of implementing a bend (0-90°) were investigated. Finally, a 90° configuration was used to test the thermal performance of a heat pipe when the location of this bend was moved further from the condenser. Experimental methods, data reduction and results will follow this section.

Nine variants of an experimental test rig were designed and manufactured to evaluate the thermal performance of a set of heat pipes in SHS and MHS configurations. This experimental set up is presented in figure 2, which included:

- A set of commercial 400 mm long × 6 mm diameter concentric tube, Wakefield-Vette copper heat pipes (WKV part number: 124656). Each heat pipe comprised a 0.5 mm thick copper housing, a 0.8 mm thick sintered copper wick (99.5% trace metals basis) and had a filling ratio of 20%.
- Two blocks of polyurethane insulation with machined slots for five evaporators and heat pipes (Note: the polyurethane material featured a nominal thermal conductivity of less than 0.05 W/m.K). One insulation block had pipe configurations for bend angles of 0°, 30°, 60° and 90° degrees, which are denoted by MHS-0, MHS-30, MHS-60 and MHS-90 respectively. For these configurations, the bend was located at the midpoint between the condenser and the first evaporator. The other block of insulation featured a range of bend locations for a 90° bend. As seen in figure 2, the first term after 90 in the configuration description represents the number of evaporators on the condenser side of the bend. For example, MHS-90-1_4 represents the configuration where there is one evaporator on the condenser side of the bend and four after.
- Four locking pins and locknuts to ensure optimum and consistent insulation of the experimental evaporator sections.

- Five copper saddles with 6 mm diameter machined grooves to achieve thermal contact with the heat pipe. A 15 mm x 55 mm Omega KHLV (part number: KHLVA-105/5-P) resistive heater mat was attached to each saddle to act as a heat source (see figure 5). The rig was designed to test one heat pipe at a time, and there was a minimum insulation distance of 25 mm between components and edges to minimize heat exchange between saddles. Thermal adhesive paste (Dowsil™ /Dow Corning 304 Heat sink Compound, thermal conductivity 0.67 W/m.K as per the supplier's data sheet) was used to reduce the thermal contact resistance at the interface between the copper saddles and the heat pipe.
- Three EL302RT Aim-TTi bench power supplies were used to power the Omega heater mats and condenser's pump.
- A 100 mm diameter x 70 mm long stainless steel 304 cylinder configured as a calorimeter [23]. The cylinder featured a fully drilled through 6.1 mm diameter hole, axially along its centerline, for snug fitting of the heat pipe. Dowsil™ Thermal adhesive paste was also used to reduce the thermal contact resistance at the interface between the calorimeter and the heat pipe. The condenser calorimeter was surrounded by a 6 mm copper coil which carried a coolant, silicone oil, at a controlled temperature (15 °C) that was regulated using a Huber Ministat 125 water bath. An M500 TTS Micro Series pump was used to circulate the coolant from the isothermal bath through plastic tubing to the copper coil. The condenser section was insulated using machined fit polyurethane insulation in order to isolate heat transfer to the cooling coil.
- 32 K-type thermocouples were calibrated to ± 0.1 K uncertainty in a Huber Ministat waterbath against a Fluke 5610 reference thermistor probe (uncertainty ± 0.01 K). The thermocouples were attached to the heat pipe and evaporator surfaces as seen in figure 3.a. A combination of thermal adhesive paste and copper foil tape was used to minimize potential uncertainties associated with interfacial thermal resistance between the thermocouples and the heat pipe and calorimeter block.
- A National Instruments 32 channel thermocouple NI TB-4353 module was used to connect 32 RS Pro K type thermocouples (RS Stock No. 363-0250) to a National Instruments NI PXIe-1082 data recorder with LabView software.

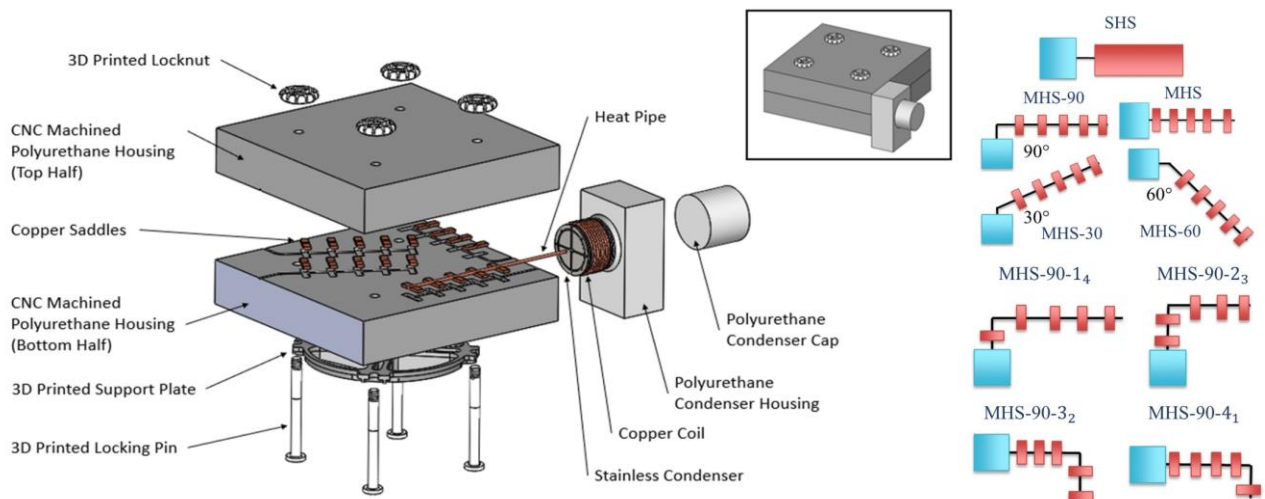


Figure 2: MHS experimental apparatus including configurations to examine the effects of bend angle and location.

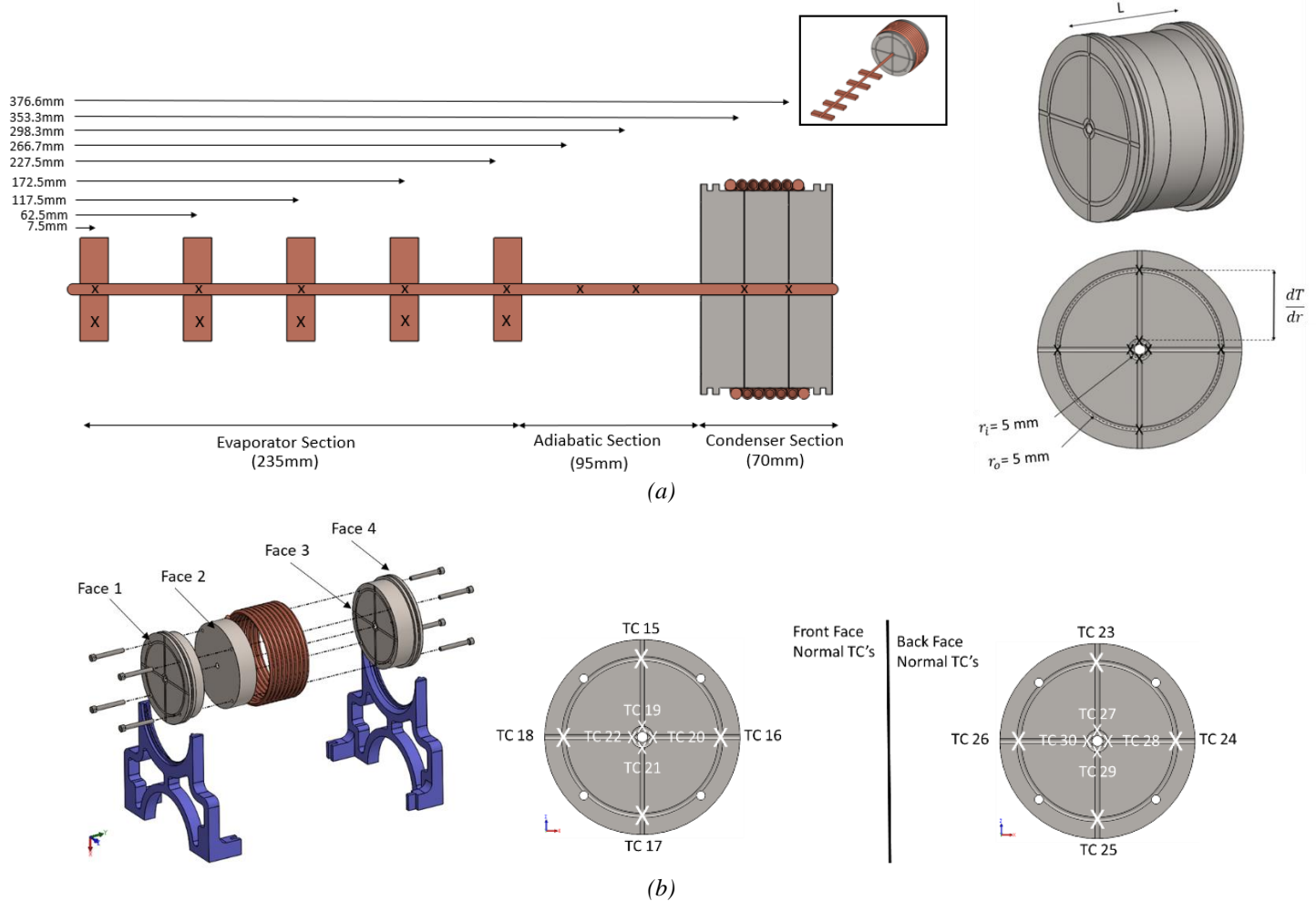


Figure 3: MHS configuration and thermocouple locations. 'X' denotes the location of the thermocouple. (a) Heat pipe thermocouple locations. (b) Condenser assembly and thermocouple locations. Inner thermocouples are considered closer to the centre.

The first set of experiments tested the performance of an MHS configuration with a range of bend angles (0° , 30° , 60° and 90°) in the heat pipe. The locations of the thermocouples on the heat pipe copper saddles and condenser are highlighted in figures 3 (a) and (b) respectively. These locations were kept consistent for all tests detailed in this paper and can be identified in figure 3 by the mark 'X'. Five thermocouples were placed on the copper saddles, and five more were placed on the heat pipe evaporator sections, directly above the copper saddles, see figure 3 (a), to calculate an average evaporator temperature (\bar{T}_e). Two further thermocouples were placed on the adiabatic section, and two more on the condenser section, to calculate an average condenser temperature (\bar{T}_c). This thermocouple configuration was replicated from a previous study [18], in which the effects of equal and unequal heat loads for straight MHS configurations were investigated.

In order to calculate heat transferred out of the condenser section, sixteen thermocouples were embedded into 15 mm deep, 1 mm diameter holes from the center of both faces of the condenser at marked the locations, see figure 3 (b). The outer and inner radii for the thermocouples were 45 mm and 5 mm respectively, see figure 3 (a). Two thermocouples were used to

measure the ambient air temperature and the temperature of the silicon oil coolant.

Figure 4 outlines the location of the bend and how the angle was measured. All pipes had a bend radius of 20 mm. Locations 1–4 illustrate the location of the 0° – 90° bends. For the analysis of the effect of bend location, the bend was located at the midpoint between the evaporators. The locations of these five bends can be seen in figure 4 with the mark 'O'. Points 5–8 represent the different locations of the bends that tested an MHS 90° bent heat pipe.

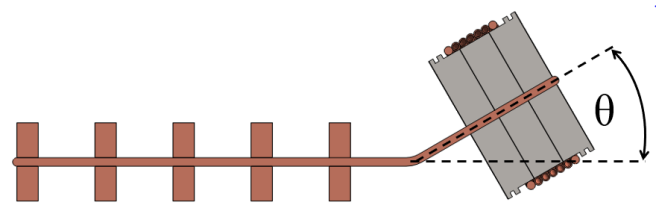


Figure 4: Heat pipe bend angle & bend location denoted by 'O'.

The copper saddles were made from a number of small copper blocks which were machined with a $\text{Ø}6\text{ mm}$ ballnose cutter to create copper saddles for the heat pipe (see figure 5). As shown in figure 5, the electrical heater mat was attached using double-

sided thermal tape to the underside of the copper saddle. Thermal paste was placed between the heat pipe and the copper saddle groove to minimize contact resistance.

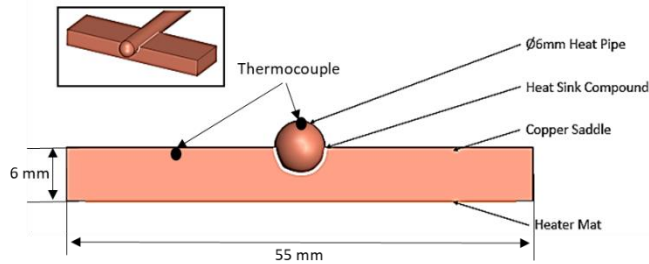


Figure 5: Copper saddle heat source configuration.

In order to provide a baseline, a straight heat pipe in an SHS configuration was also tested, as shown in figure 6. This consisted of a single copper saddle spanning the entire evaporator section. The copper saddle dimensions were 235 mm × 55 mm × 6 mm, with a Ø6 mm groove through the middle. For consistency, K-type thermocouples had the same locations as shown in figure 3. The ancillary equipment was configured in a similar manner to the MHS rig, figure 3, which is outlined in the top right corner of figure 6.

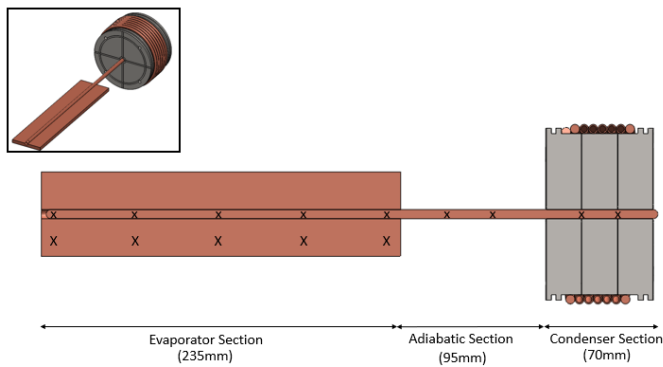


Figure 6: SHS configuration with individual copper saddle acting as a uniform heat source.

III. EXPERIMENTAL METHOD

The experimental rig was assembled and connected to all ancillary equipment as shown in figure 7. When a steady state temperature of 15°C in the thermocouples located at outer ring of the calorimeter block was achieved, the data recorder was started and the power supplies to the heater mats were switched on to specific power inputs. The system was allowed to reach steady state for each power input, defined as a change of less than 0.5 °C in 30 minutes in all the thermocouples. Once this was reached, the power was stepped up in intervals of 5 W for the SHS configuration, or 1 W per heater element for MHS, until the final power input was achieved, at steady state. Once complete, the data logger was stopped, and the data stored.

The experiment tested power inputs over the range of 5 W to 30 W in increments of 5 W. Temperature readings were recorded over time. If any of the copper saddles reached a temperature of above 96 °C the heat pipe was assumed to have reached its limit and the experiment was stopped. Steady state temperature readings were averaged over the last 10 minutes and used for experimental calculations. To ensure consistency, all heat pipes were initially tested in a straight configuration. The heat pipes had to be within ±5% for all heat inputs in the straight SHS configuration before use in any other configuration. Thereafter, each configuration was tested with three different heat pipes and tests for each heat pipe were repeated twice. The thermal performance of the heat pipes had to be within ± 5% of the configuration's average to be deemed suitable for further investigation.

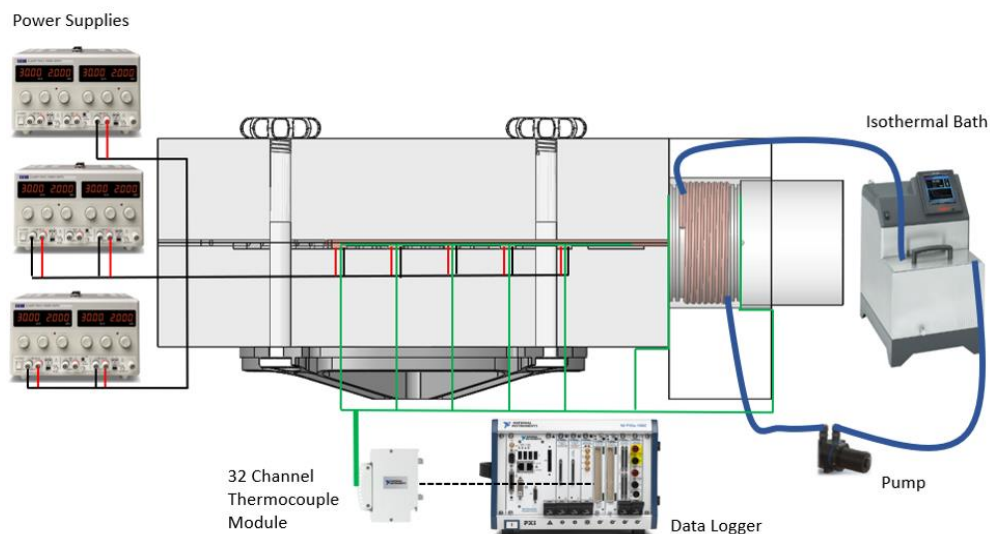


Figure 7: Cross section side view of MHS experiment equipment.

IV. EXPERIMENTAL DATA REDUCTION

Thermal resistance (R_{th}) and the equivalent effective thermal conductivity (k_{eff}) were calculated to evaluate the thermal performance of the various configurations of heat pipes. The power supplied (P_w) to each heater mat was determined from equation 1:

$$Q_{in} = P_w = VI \quad 1$$

Where, Q_{in} is the heat supplied to the evaporator and, V and I are the voltage and current supplied to the heater mat via the power supply respectively.

Heat pipe thermal resistance and effective thermal conductivity were calculated using equations 2 and respectively. An overall thermal resistance was used because the heat pipes were considered to be part of an individual system with a single condenser [18, 24]. Thus, the average heat pipe temperature across the single (SHS) and five (MHS) evaporators, \bar{T}_e , was used when calculating thermal resistance. This was achieved by averaging the five surface temperatures along the evaporator of the heat pipe.

$$R_{th} = \frac{\bar{T}_e - \bar{T}_c}{Q_{in}} \quad 2$$

$$k_{eff} = \frac{L}{R_{th} \cdot A} \quad 3$$

Where, \bar{T}_c is the average condenser temperature of the heat pipe, Q_{in} is the sum of the heat input from all five evaporators (equation 1), L is the length between the center of the evaporator section and the center of the condenser section [18, 24], and A is the cross sectional area of the heat pipe.

The maximum uncertainties in each quantity calculated in equations 1–3 were obtained using the method of Kline and McClintock [25] for constant odds results, using the root-sum-square contribution of the individual contributions of the variables (equation 4). Where ΔZ was the uncertainty (\pm) in the derived quantity $Z = f(x_1, x_2, x_3 \dots x_N)$, and Δx_i was the uncertainty (\pm) in the primary variable x_i . The uncertainty ΔZ was then calculated as:

$$\Delta Z = \sqrt{\sum_{i=1}^N \left[\frac{\delta Z}{\delta x_i} \Delta x_i \right]^2} \quad 4$$

For the experimental uncertainty analysis, the voltages and currents supplied to the copper saddles were calibrated using a Fluke 175 True-RMS digital multimeter against three EL302RT Aim-TTi bench power supplies; the uncertainties in voltages and currents were ± 100 mV and ± 10 mA, respectively.

It is evident from equation 2 that the uncertainty in the thermal resistance of the heat pipe depends on the uncertainties in Q_{in} and in the thermocouples attached to the surface of the heat pipe. Thermocouples were calibrated to ± 0.1 K using a Huber Ministat 125 water bath where a Fluke 1504 temperature reference probe (uncertainty ± 0.002 K at 298 K), and a Fluke 5610

secondary reference thermistor probe (uncertainty ± 0.01 K) were used as references.

The dominant uncertainty in effective conductivity was that associated with thermal resistance. There were, however, additional uncertainties associated with the length and diameter of the heat pipe. The spatial uncertainties with the machined parts were all within ± 0.05 mm, and the manufacturer specification and Vernier precision of the length and diameter of the heat pipes was ± 0.1 mm.

With reference to the calorimeter block, the dimensional uncertainty in the radial (Δr) and longitudinal (Δl) axes was ± 0.05 mm. For the stainless steel 304 block used to quantify the flow of heat within the calorimeters, the thermal conductivity (k) was quoted with an uncertainty of less than $\pm 2\%$ for all temperatures used in this study. The steady-state measurements for thermal conductivity of the calorimeter blocks were recorded and used for the accurate quantification of Q_{out} . However, Q_{out} was not used in the analysis of R_{th} and k_{eff} . Maximum uncertainties in Q_{in} , k_{eff} , Q_{out} and all measurements of R_{th} (see R_{th_e} and R_{th_s} in section V) were found to be $\pm 4.0\%$, $\pm 7.3\%$, $\pm 5.1\%$, and 6.3% , respectively.

V. RESULTS AND DISCUSSION

Section V.A starts by identifying the effect of implementing an MHS setup and a bend on a heat pipe that was tested for SHS thermal performance measurements. Following this, section V.B addresses the effect of changing the bend location in an MHS heat pipe. Subsequent discussion details the influence of changing the bend location, for the MHS configurations. All comparisons include results of thermal resistance of the heat pipe, local heat pipe and copper saddle nominal thermal resistance, total heat pipe effective thermal conductivity, and maximum heat input.

A. Effect of Bend Angle for an MHS Heat Pipe

Figure 8 presents the thermal resistances of the baseline SHS heat pipe configuration and the MHS heat pipe as a function of heat input for a range of bend angles. It is evident that the R_{th} of the heat pipes tested in the current study reduces as Q_{in} increases for both SHS and MHS cases. This trend is consistent with previously published results, and it occurs because an increase in Q_{in} accelerates the vaporization of the working fluid in the evaporator(s). This results in an increase in vapor pressure within the vapor lines forcing the vapor to condense more rapidly in the condenser. The capillary pressure difference between the pore space of the condenser and the evaporator(s) also increases, which increases the liquid mass flow rate and reduces the total thermal resistance. However, with a further increase in Q_{in} , only a slight decrease occurs in the thermal resistance of the heat pipe. It can be seen from figure 8 that changes to the evaporator configuration or geometry of the heat pipe, like MHS and a bend, affect the evaporation-condensation cycle in the heat pipe and, thus, increase the thermal resistance. For example, the thermal resistance of the straight MHS set up increased by up to $\sim 70\%$ in comparison to its SHS counterpart. Similarly, the thermal performance of the heat pipe was significantly reduced when bent from $0-90^\circ$ for all heat

inputs. At low heat inputs, 10 W, the thermal resistance of an MHS set up increased from 0.355 K/W at 0° to 0.477 K/W at 90° (~26%) and for higher heat inputs of 25 W, thermal resistance increased from 0.229 K/W at 0° to 0.380 K/W at 90° (~65%). This result was similar to that reported by [4], where an increase in thermal resistance of ~22% was reported as the bend angle increased from 0° to 90° for an SHS configuration. However, the overall increase in thermal resistance, as the configuration was converted from SHS to MHS with 90° bend (MHS-90), was far greater than recorded by previous work for just an individual SHS with bends [4] and an straight MHS without a bend [18]. Overall, there was an increase of ~114% (for 5 W) to 200% (for 25 W) in the thermal resistance of the pipes.

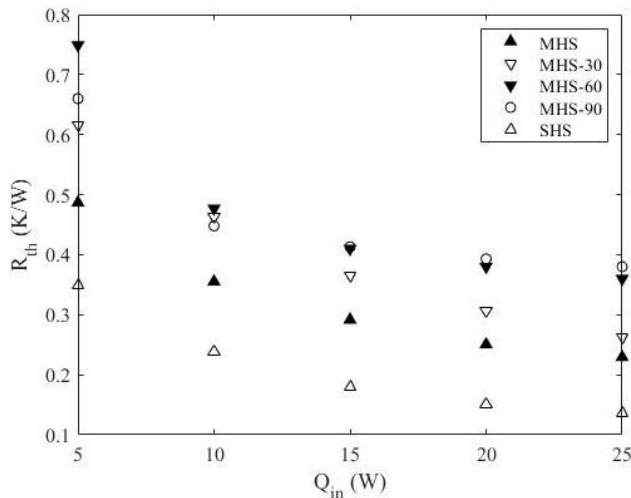


Figure 8: Thermal resistance as a function of total heat input for SHS, MHS, and bent MHS configurations.

This study presents information on how the implementation of an MHS and a bend into an application can have an adverse effect on thermal performance. As seen in figure 8, the overall thermal resistance of the heat pipe is greatly increased by these measures. However, these values represent the average thermal resistance of five evaporators. To gain a deeper understanding as to why the thermal performance of a bent MHS heat pipe decreases, the nominal local evaporator thermal resistance for each heat pipe configuration is presented in figure 9. Nominal evaporator resistance was calculated by dividing the difference in the local evaporator (T_e) and average condenser temperatures of the heat pipe by the local heat input. i.e., ($R_{th,e} = T_e - \bar{T}_c / (0.2 * Q_{in})$). Only one Q_{in} , 15 W, value was considered because similar trends in the local thermal resistance were observed throughout. As expected, the $R_{th,e}$ measurements for the SHS configuration remain lowest while exhibiting near isothermal conditions, in the range 0.19 – 0.22 K/W. The MHS configuration, on the other hand, does not exhibit the same isothermal conditions. In this configuration, the resistance of the evaporator furthest from the condenser (7.5 mm) is 35% higher than that of its neighboring evaporator and ~15% higher than its R_{th} . This trend in the MHS $R_{th,e}$, however, is altered further when the pipe is bent. For example, the MHS-30 and MHS-60 configurations exhibit a maximum thermal resistance at the

evaporator located 60 mm from the evaporator end. Whereas the maximum thermal resistance for the MHS-90 occurs at the evaporator closest to the condenser, with evaporator resistances gradually reducing towards the evaporator end before increasing to give a 30% difference between the first and last evaporators.

The non-monotonic trends in $R_{th,e}$ evident in figure 9 for both SHS and MHS cases may have been caused by several reasons related to the configuration of the heat pipe and its effect on the fluid transport mechanisms, as well as discrete variations due to the manufacture and implementation of the heat pipes into the apparatus. In particular, the interfacial resistance between the heat pipe and copper saddles could give rise to this variation, however, a highly conductive thermal paste was used at the interface to minimize this resistance. Moreover, the evaporator thermal resistance may have varied along the length of the pipe due to manufacturing inconsistencies which include: a potential lack of contact between the wick and pipe housing; local variations in the porosity of the wick; impurities in the copper; and non-condensable gases (NCG) in the working fluid being retained in the condenser (see section V.D for further discussion). Hence, local variations in $R_{th,e}$ are believed to be partially related the mounting of the heat sources in the configuration, and to the heat pipes used. As outlined in Section III, the thermal performance of the heat pipes tested had to be within $\pm 5\%$ of the configuration's average to be deemed suitable for further investigation in this study. As such, any discussion on evaporator thermal resistance is focused on the transport mechanisms inside the pipe.

It is postulated that the rise in $R_{th,e}$ from an SHS to an MHS case was caused by greater axial fluxes at the evaporators increasing the vapor pressure at the liquid-vapor interface, amongst other aspects. It is clear from figure 9 that the trend in $R_{th,e}$ of the heat pipe changes from MHS to MHS-30 and MHS-60. It is speculated that the greater bend angle increases the fluidic pressure losses around the bend. Consequently, driving pressure of the liquid to the final two evaporators (7.5 mm and 62.5 mm) is diminished which results in higher values of $R_{th,e}$, an indication that the pipe is approaching its capillary limit. Finally, the MHS-90 heat pipe exhibits a gradual reduction in $R_{th,e}$ from the condenser to the evaporator end, yet the highest values of $R_{th,e}$ are observed. It is postulated that capillary and entrainment effects are occurring, and a restriction in the vapor passage in the bent adiabatic section is adding to an increased vapor pressure at the liquid-vapor interface of the nearby evaporators [26]. Further discussions related to bend angle, and the capillary and entrainments limits, are presented in section V.D.

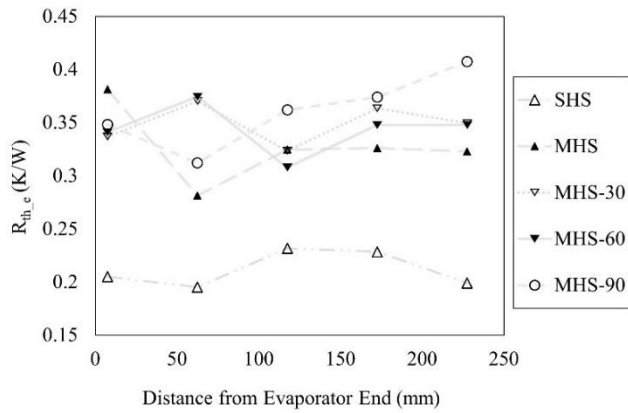


Figure 9: Nominal thermal resistance of the evaporators as a function of distance from the evaporator end for all MHS bend angles. SHS is presented as a baseline. Where, $Q_{in} = 15$ W.

Figure 10 illustrates the thermal resistances at the copper saddle (or ‘circuit component’) as a function of the distance from the evaporator end of the heat pipe, for $Q_{in} = 15$ W. Nominal saddle thermal resistance was calculated in a similar manner to the local evaporator thermal resistance, but where the surface temperature of the evaporator is replaced with the internal temperature of the corresponding copper saddle ($R_{th,s} = T_s - \bar{T}_c / (0.2 * Q_{in})$). It is clear from figure 10 that the SHS saddle maintains a similar isothermal state as the evaporators because no additional variables have been added to the cooling solution, i.e., an MHS and a bend. In contrast, the MHS, MHS-30 and MHS-60 saddles display a near concave trend, with the extreme saddles showing the highest resistances. It is postulated from figure 10 that the MHS, MHS-30 and MHS-60 heat pipes impose a less restrictive path to the liquid / vapour phases within the heat pipe, in contrast to the MHS-90 heat pipe. Hence, the heat sources furthest from the condenser have a larger quantity of liquid available for effective evaporation. It is evident from the MHS-90 the evaporation-condensation cycle is disrupted when a heat pipe is bent. It is speculated that the 90° bend imposes local liquid flow restrictions that reduce the effective liquid driving pressure after the bend. Hence, greater fluid evaporation occurs at the saddles closest to the condenser, reducing the liquid available to the later saddles.

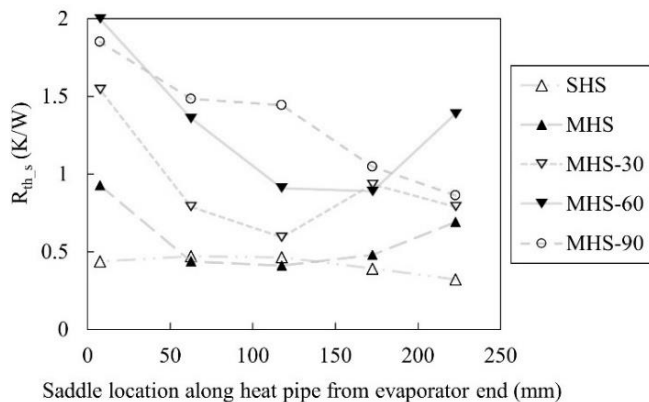


Figure 10: Copper saddle thermal resistance as a function of location from the evaporator end of the heat pipe: 0 mm indicates the distance furthest from the condenser. Where, $Q_{in} = 15$ W.

B. Effect of Bend Location for an MHS Heat Pipe

From the configurations presented in section V.A, it is now evident that introducing a bend into an MHS heat pipe greatly reduces thermal performance. However, little to no information is known on the effect of the location of the bend along an MHS heat pipe. Figure 11 illustrates the influence of the location of a 90° bend between evaporators. The bend location was varied along the heat pipe to yield different numbers of evaporators on either side of the bend. Figure 11 shows that changing the location of the bend influences the thermal resistance of the heat pipe. Depending on the thermal load, the thermal resistance increases by between 5 to 18%. In fact, the configurations with the lowest thermal resistance are the MHS-90-2₃ for $Q_{in} \leq 15$ W and MHS-90-4₁ for $Q_{in} > 15$ W, whereas the configuration with the highest average thermal resistance was MHS-90-1₄ (11-18% reduction in average thermal resistance compared to an MHS-90).

It is apparent from figure 11 that bend location in an MHS heat pipe is influential in determining thermal performance, where the change in thermal performance is likely due to restrictions imposed on the fluid flow. Shabgard and Faghri [27] demonstrated that the liquid and vapor velocities along an MHS heat pipe are a function of the distance from the evaporator and condenser ends of the heat pipe. Specifically, vapor velocities and liquid flux are expected to be at a maximum between the condenser and its closest evaporator. It is postulated that the MHS-90 and MHS-90-1₄ configurations have the highest thermal resistances at $Q_{in} > 15$ W because the vapor velocities and the returning liquid flux are highest at the bend site. It is likely that the fluidic pressure losses around the bend are a maximum, imposing a greater contribution to the capillary limit of the heat pipe. Furthermore, higher vapor velocities increase the interfacial shear stresses at the liquid-vapor interface, possibly giving rise to entrainment. In contrast, the MHS-90-2₃ heat pipe was less severely affected by the bend. In this arrangement the location of the bend closer to the evaporator end ensures vapor velocities (i.e., interfacial shear stresses) were lowest at the bend, where entrainment is less likely to occur. Hence, it is postulated that the entrainment limit may be adversely affected by bend location in an MHS heat pipe, and this is discussed further in section V.D.

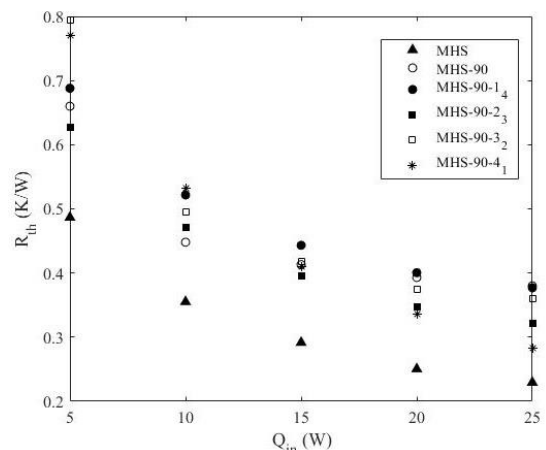


Figure 11: Thermal resistance as a function of total heat input for MHS, MHS 90° bend, and MHS with a range of bend locations.

Figure 12 illustrates the local evaporator thermal resistance for all 90° configurations, for a range of bend locations, and for $Q_{in} = 15$ W. The MHS is used as a base for this analysis. On average, the MHS-90-2₃ and MHS-90-4₁ configurations have the smallest rise in thermal resistance in comparison to the MHS configuration, of 8-16% and 12-38% respectively. The MHS-90-1₄ and MHS-90-3₂ configurations, on the other hand exhibit the largest rises in thermal resistance, of 19-52% and 22-56% respectively. The latter, lower performing configurations portray a relatively uniform high thermal resistance throughout the evaporators. For the configurations which incur a sharp increase in thermal resistance (MHS, MHS-90-2₃ and MHS-90-4₁), it is postulated that fluid flow is restricted, i.e., MHS dry-out or liquid impediment due to bending. The configurations with uniformly high resistance imply that the MHS and bend location are both affecting the performance of the heat pipe.

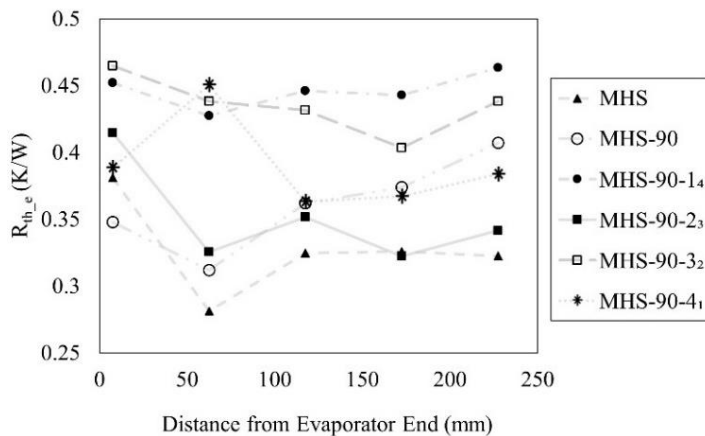


Figure 12: Nominal thermal resistance of the evaporators as a function of distance from the evaporator end for all MHS bend locations. MHS is used as a base. Where, $Q_{in} = 15$ W.

Figure 13 illustrates the thermal resistances of the five copper saddles for the various 90° bend location configurations. The effective cooling of the heat pipe significantly changes between configurations. The plot shows that the MHS and MHS-90-4₁ heat pipe features a similar trend in saddle thermal resistance because their configurations are similar, i.e., a concave trend with the highest resistances recorded at the 7 mm and 230 mm saddles. There is, however, a much larger difference between the resistances at the 60 mm and 7 mm saddles for an MHS-90-4₁, from ~1 K/W at 60 mm to ~1.9 K/W at 7 mm. It is assumed for the MHS-90-4₁ heat pipe that the increase occurs because of the impediment of the working fluid at the bend, which is beside the last saddle.

An additional feature of the bent MHS heat pipes is evident in the saddle resistances of the MHS-90-2₃ and MHS-90-3₂ configurations. As presented in figure 13, there is a significant difference in thermal resistance between the copper saddles located at either side of the bend. The MHS-90-2₃ heat pipe has a ~80% difference between the two saddles furthest from the condenser, at 7 mm and 60 mm, and the other three located closest to the condenser. The MHS-90-3₂, on the other hand, has a ~40%,

difference between the same 7 mm and 60 mm saddles, showing that, in this configuration, the thermal resistances of the five evaporators are more uniformly affected by the location of the bend.

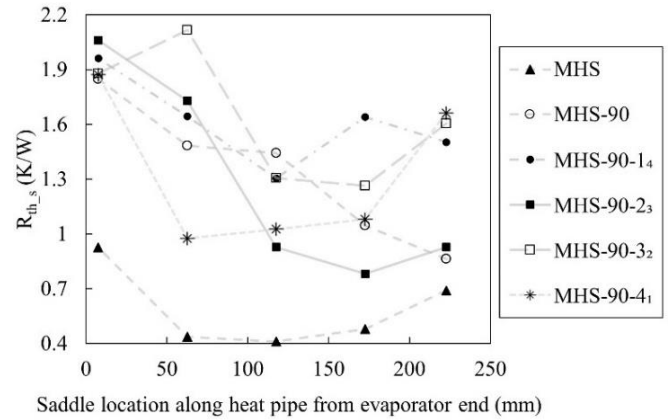


Figure 13: Copper saddle thermal resistance as a function of location from the evaporator end of the heat pipe for the various 90° bend location configurations. 0 mm indicates the distance furthest from the condenser. Where, $Q_{in} = 15$ W.

C. Effective Thermal Conductivity and Maximum Heat Input

Effective thermal conductivity (k_{eff}) is a useful parameter to compare pipes of similar dimensions. Figure 14 presents effective thermal conductivity as a function of heat load and test configuration. As thermal conductivity is inversely proportional to the thermal resistance of the heat pipe (see equation 3), figure 14 illustrates the overall drop in thermal conductivity (i.e., increase in thermal resistance) from an SHS to an MHS configuration with a 90° bend.

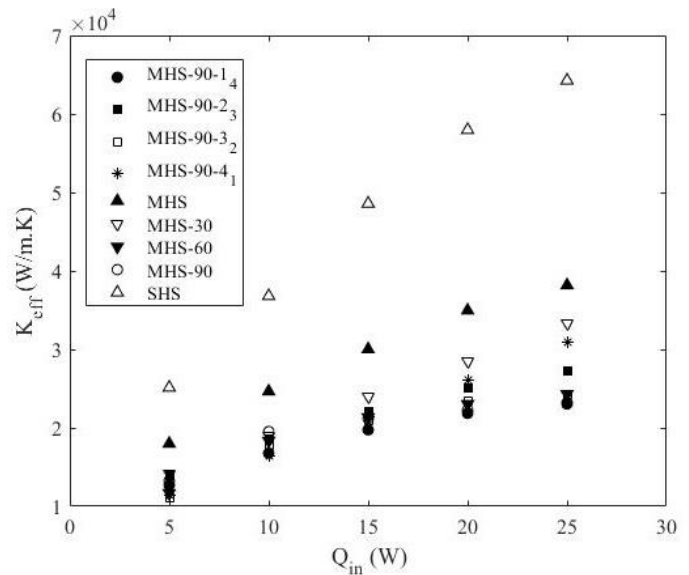


Figure 14: Effective thermal conductivity of a heat pipe as a function of total heat input from SHS to MHS with bend angle and location included.

Figure 15 presents the total maximum heat input (Q_{max}) of the heat pipes for all the configurations tested. Q_{max} was assumed to occur when the difference in the evaporator temperatures was $> 2^{\circ}\text{C}$, an indication of the onset of dry-out. The respective effects of bending angle and location of a 90° bend on the capillary limit of an MHS heat pipe are presented in figure 15, on the top and bottom x-axes. It can be seen that the top left-hand corner represents the highest performing configuration, which was the SHS heat pipe, at $Q_{max} = 30 \text{ W}$. The figure also demonstrates that a higher bending angle in the adiabatic region of an MHS heat pipe, and bend locations further from the evaporator end of the heat pipe, both reduce Q_{max} . The MHS configuration has an $\sim 11\%$ lower Q_{max} in comparison to its SHS counterpart, postulated to be a result of higher liquid flux demands that reduce the capillary limit of the heat pipe. As expected, bending the MHS heat pipe from $0-90^{\circ}$ reduces Q_{max} by an additional $\sim 17\%$ which represents the maximum reduction in Q_{max} for all bend configurations. It is postulated that the configurations with the bend located closest to the evaporator end (145 mm, 90 mm, and 35 mm) are dominated by capillary limitations. In contrast, the configurations with the bend located furthest from the evaporator end (200 mm and 270 mm) are likely to be affected by both capillary and entrainment limitations. Further discussions of these phenomena can be found in section V.D.

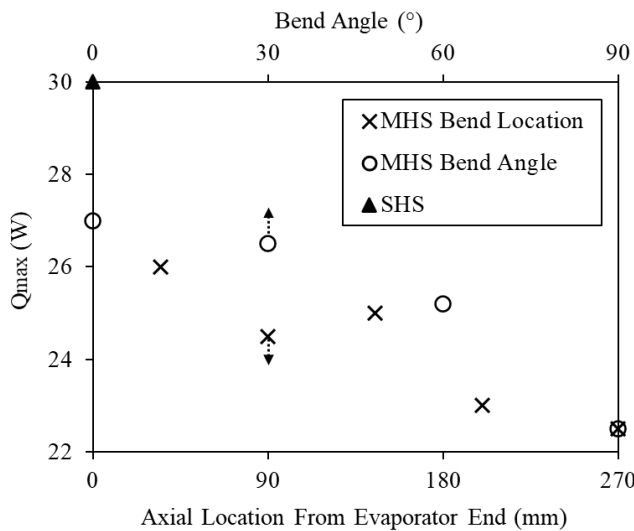


Figure 15: Q_{max} as a function of the heat pipe bend angle and axial location of a 90° bend from the evaporator end. Note: Arrows in graph indicate the reference x-axis for the data series.

D. Comparison of SHS, MHS and MHS with a Bend

Figure 16 illustrates the various phenomena occurring in the bent MHS heat pipes which are expected to contribute to the reduction in thermal performance. When the liquid phase within the wick reaches a heat source, it starts to evaporate. If the heat flux at this source is minimal, sufficient fluid can pass the source and flow to the next. However, if the quantity of liquid return within the wick is too low, or if the heat flux is too high, the liquid can evaporate and start to dry-out the wick as it passes from one evaporator to the next. Data for the total heat flux of an SHS and

an MHS configuration are presented in table 1. It is evident that the total radial heat flux is ~ 15 times higher for the MHS configuration, compared to the baseline SHS. From previous studies [4, 17], it is postulated that the rate of evaporation is higher in an MHS heat pipe, resulting in insufficient fluid reaching the furthest heat source from the condenser section, as illustrated in figure 16. Hence, the heat pipe does not effectively cool the latter saddles, as demonstrated from the data in figures 10 and 13. Consequently, the average temperature of the copper saddles increases. It is also possible that the radial conductive thermal resistance in the wick varied between configurations. Poorer thermal contact between the wick and housing, or cracks in the wick, can reduce thermal transport to the liquid-vapor interface, thus lowering effective evaporation and increasing $R_{th,e}$. It is postulated from figures 9 and 12 that there were discrete differences in the evaporator thermal resistance that caused the non-monotonic nature of $R_{th,e}$ for the straight SHS and MHS heat pipes. This phenomenon is likely to also influence the bent MHS heat pipes. Moreover, it is assumed that the higher $R_{th,e}$ (or T_e) values had a secondary, adverse effect on the vapor pressure at the liquid-vapor interface which could contribute to a reduction in Q_{max} .

Table 1: Total heat flux for a SHS and MHS heat pipe. Note that the heat fluxes for MHS heat pipe and copper saddle are the sum of the five evaporators. Hence, the flux should be divided by five to find the heat flux of one evaporator.

Q_{in} (W)	Heat Flux SHS (W/m ²)		Heat Flux MHS (W/m ²)	
	Pipe Contact Area ($\times 1$)	Copper Saddle ($\times 1$)	Pipe Contact Area ($\times 5$)	Copper Saddle ($\times 5$)
5	2257	386	35367	6060
10	4515	773	70736	12120
15	6772	1160	106103	17790
20	9030	1547	141470	24240
25	11288	1934	176838	30300

Another aspect to consider is the effect of bend angle on the internal geometry of a heat pipe. Post experimentation, a heat pipe was cross-sectioned using a pipe cutter at the bend site. Images of the cross section obtained using a microscope are presented in figure 17. Heat pipes operate on the balance of capillary pressure with the opposing vapor, liquid and gravitational pressure drops, i.e., the capillary limit [28, 29]. If any of these pressures increase, then the thermal performance of the heat pipe is affected [21, 22, 30]. From figure 17, it is evident that vapor channel and wick deformation occur in the bent heat pipes. This could lead to local restriction of the vapor channel causing the vapor flow to accelerate and increase the pressure drop in the gaseous phase around the bend. Any rise in the vapor pressure drop can have minor contributions to lowering Q_{max} (i.e., capillary limit) of the heat pipe and eventually dry-out [21, 22]. However, the liquid pressure drop is considered to have a significant impact on the capillary limit of a heat pipe in comparison to the gaseous phase [30].

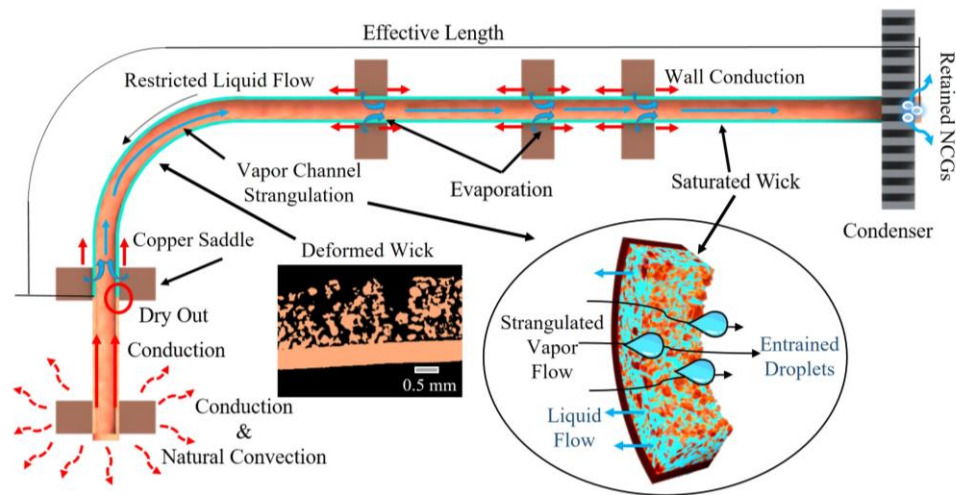


Figure 16: An illustration of the potential limiting factors of a bent MHS heat pipe. Note that in this scenario all liquid has evaporated before it passes the second last evaporator, and droplets are entrained from the wick where the vapor flow is restricted. Furthermore, a buildup of NCGs in the condenser can cause a drop in the average condenser temperature.

It is known that the liquid pressure drop in a wick is inversely proportional to the porosity of the wick [28, 29, 31]. From figure 17, it is clear that local reductions in wick porosity could exist due to buckling of the copper particles. This change in porosity will have an adverse effect on the liquid pressure losses inside the heat pipe. These observations, however, are only postulated on the basis of a single destructive cross-section of the heat pipe. If more detailed information about these phenomena is required, another, non-destructive method of analyzing the heat pipe in three dimensions is required. Nevertheless, targeted manufacturing steps to minimize deformations of the restricted vapor channel and wick structures of a bent heat pipe would be advantageous in terms of minimizing any additional pressure drops.

The experimental analysis in this study has shown that the thermal performance of a bent MHS heat pipe is a function of bend location and Q_{in} . The vapor and liquid velocities play significant roles in the evaporation-condensation cycle of an MHS heat pipe, and also influence the limits of operation, particularly the capillary and entrainment limits. The effect of bending on the capillary limit has been previously discussed. However, entrainment may also influence the thermal performance of a bent MHS heat pipe, particularly when the bend location is changed. Entrainment occurs when the vapor velocity in the heat pipe is sufficiently high to shear liquid from the wick. The relevant dimensionless number that determines entrainment is the Weber number, which is the ratio of inertial vapour forces to liquid surface tension forces:

$$We = \frac{\rho_v v_v^2 h_{l-v}}{2\pi\sigma_l} \quad 5$$

Where, ρ_v , v_v , h_{l-v} , and σ_l are the vapor density, vapor velocity, hydraulic height of the liquid-vapor interface, and surface tension of the liquid, respectively. Entrainment is assumed to occur when We is of order 1.

From figure 11, it is clear that the MHS-90 and MHS-90-1₄ configurations are the poorest performing heat pipes at $Q_{in} > 15$ W, where the bend is located closer to the condenser end. MHS heat pipe behavior suggests that vapor velocities are lowest at the evaporator end and increase as the vapor travels to the condenser, passing heat sources in the process. Hence, locating the bend closer to the condenser would imply that higher vapor velocities, i.e., viscous shear forces, are encountered at the bend site. In contrast, the liquid flux in the wick is at a maximum near the condenser end and depletes along the heat pipe as it is evaporated, where it is assumed that h_{l-v} is proportional to liquid flux. The Weber number evokes a proportional relationship for v_v^2 and h_{l-v} . It is postulated that locating the 90° bend further from the condenser end results in diminished values of v_v and h_{l-v} at the bend

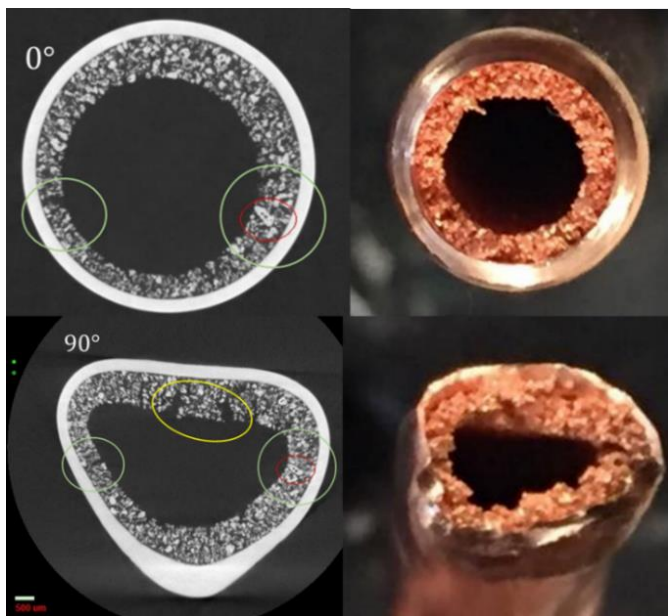


Figure 17: Images of cross-sections in a straight heat pipe and a heat pipe bend at 90°.

site, thereby minimizing entrainment effects. Note that entrainment may only be an issue for higher values of Q_{in} and must be considered. For example, in section V.B the MHS-90 heat pipes with the bend located closer to the condenser end perform best at $Q_{in} < 15$ W. It is speculated that, in these scenarios the Weber number may reduce below 1 and thus other factors may dominate the thermal performance degradation of the MHS-90 heat pipe, such as capillary limitations.

VI. CONCLUSIONS

Quantitative differences in performance between heat pipe configurations were collected experimentally in terms of thermal resistance, heat pipe evaporator thermal resistance local to the copper saddles, saddle thermal resistance, and effective thermal conductivity. This study concludes that the performance of the heat pipe deteriorates as: the pipe's evaporator configuration changes from a single heat source (SHS) to multiple heat source (MHS); a bend is induced between the condenser section and evaporator section in a MHS configuration; the bend angle is increased to 90° ; and the location of the 90° bend is changed along the axis of the MHS heat pipe, i.e., between different evaporators. The SHS heat pipe is used as a baseline comparison for all configurations, the MHS configuration is used to act as a baseline for comparing bend angle and location, and the MHS-90 heat pipe is used to assess the influence of changing bend location on the performance of the heat pipe.

For the SHS to MHS analysis, it is seen that thermal resistance increases by 26-65% for power inputs ranging from 5 to 25 W. Thermal performance measurements shows an increase in thermal resistance when a heat pipe is bent, similarly to trends reported in the literature. However, for MHS configurations, measurements in thermal resistance would have underestimated the effect of a bend. Experimental results show that progressing from MHS to MHS with a 30° bend increases the thermal resistance by 15-20%, and a 90° bend increases the thermal resistance by up to 65%. It is postulated that the reasons for these increases in resistance are due to higher radial heat fluxes caused by the MHS configuration, where local liquid cooling demands are not being met due to dry-out, i.e., the capillary limit. This study also concludes that the bending process is likely to introduce impediments to both the liquid flow path in the porous wick structure and the vapor flow in the vapor channel, which impedes the capillary and possibly entrainment limits. This postulation is also relevant in the context of bend location. A further 18% increase in thermal resistance occurs when the location of the bend is changed. Moreover, it is concluded that there is a complex relationship between bend location and thermal resistance. In fact, there is an optimum location of the bend for an MHS with a 90° bend, i.e., MHS-90-2₃. This configuration has an 11-18% lower thermal resistance when compared to the worst configuration, i.e., MHS-90-1₄.

The results presented in this study can be used to evaluate MHS configurations in practical applications. It is concluded that:

- The implementation of a bend in an MHS configuration does not act in the exact same fashion as a straight single-source or multi-source structure. Therefore, a bent MHS heat pipe application should not be designed under assumptions made from straight SHS heat pipe characteristics.
- Thermal performance is altered if a bend moves from the adiabatic section to locations between multiple evaporators. It is also concluded that this location change is complex, and the location with the lowest average thermal resistance occurs when the bend is placed after two evaporators from the condenser side.

It is postulated that the heat transfer capacity and isothermal state of a bent MHS heat pipe is degraded due to higher fluidic resistances imposed by deformations to the wick and vapor channel, owing to higher capillary and entrainment losses. These effects, however, are a function of heat input and bend location. Hence, practices need to be employed in manufacturing the bend of a heat pipe so that minimal deformation occurs and that the location of the bend does not have significant effects on the heat pipes' heat transfer capacity.

ACKNOWLEDGEMENTS

This research is conducted with the financial support of Science Foundation Ireland (SFI) under Grant Number 13/RC/2077 and has been part funded by the European Regional Development Fund through the SFI Research Centres Programme.

REFERENCES

- [1] D. A. Reay and P. A. Kew, "2 - Heat Transfer and Fluid Flow Theory," in *Heat Pipes (Fifth Edition)*, D. A. Reay and P. A. Kew Eds. Oxford: Butterworth-Heinemann, 2007, pp. 29-106.
- [2] Y. Li, H.-f. He, and Z.-x. Zeng, "Evaporation and condensation heat transfer in a heat pipe with a sintered-grooved composite wick," *Applied Thermal Engineering*, vol. 50, no. 1, pp. 342-351, 2013/01/10/ 2013, doi: <https://doi.org/10.1016/j.applthermaleng.2012.07.042>.
- [3] M. Khalili and M. B. Shafii, "Experimental and numerical investigation of the thermal performance of a novel sintered-wick heat pipe," *Applied Thermal Engineering*, vol. 94, pp. 59-75, 2016/02/05/ 2016, doi: <https://doi.org/10.1016/j.applthermaleng.2015.10.120>.
- [4] N. Sangpab, N. Kimura, P. Terdtoon, P. Sakulchangsattajai, N. Kammuang-lue, and M. Murakami, "Combined effect of bending and flattening on heat transfer performance of cryogenic sintered-wick heat pipe," *Applied Thermal Engineering*, vol. 148, pp. 878-885, 2019/02/05/ 2019, doi: <https://doi.org/10.1016/j.applthermaleng.2018.10.099>.
- [5] S. V. Garimella *et al.*, "Thermal Challenges in Next-Generation Electronic Systems," *IEEE Transactions on Components and Packaging Technologies*, vol. 31, no. 4, pp. 801-815, 2008, doi: 10.1109/TCAPT.2008.2001197.
- [6] L. H. Chien and Y. C. Shih, "An Experimental Study of Mesh Type Flat Heat Pipes," *Journal of Mechanics*, vol. 27, no. 2, pp. 167-176, 2011, doi: 10.1017/jmech.2011.18.
- [7] S. Somasundaram *et al.*, "Detailed thermal resistance model for characterization of the overall effective thermal

- conductivity of a flat heat pipe," in *2016 15th IEEE Intersociety Conference on Thermal and Thermomechanical Phenomena in Electronic Systems (ITherm)*, 31 May-3 June 2016, pp. 23-29, doi: 10.1109/ITHERM.2016.7517523.
- [8] S. Launay, V. Sartre, and J. Bonjour, "Parametric analysis of loop heat pipe operation: a literature review," *International Journal of Thermal Sciences*, vol. 46, no. 7, pp. 621-636, 2007/07/01/ 2007, doi: <https://doi.org/10.1016/j.ijthermalsci.2006.11.007>.
- [9] A. Pal, Y. K. Joshi, M. H. Beitelmal, C. D. Patel, and T. M. Wenger, "Design and performance evaluation of a compact thermosyphon," *IEEE Transactions on Components and Packaging Technologies*, vol. 25, no. 4, pp. 601-607, 2002, doi: 10.1109/TCAPT.2002.807997.
- [10] R. Bruce, M. Barba, F. Bouchet, A. Bonelli, and B. Baudouy, "Transient Thermal Behavior of a Neon Pulsating Heat Pipe (PHP)," *IEEE Transactions on Applied Superconductivity*, vol. 29, no. 5, pp. 1-5, 2019, doi: 10.1109/TASC.2019.2902978.
- [11] L. Man, W. Man, and Y. Zohar, "Integrated micro-heat-pipe fabrication technology," *Journal of Microelectromechanical Systems*, vol. 12, no. 2, pp. 138-146, 2003, doi: 10.1109/JMEMS.2003.809955.
- [12] D. A. Reay and P. A. Kew, "Introduction," in *Heat Pipes (Fifth Edition)*, D. A. Reay and P. A. Kew Eds. Oxford: Butterworth-Heinemann, 2007, pp. 1-8.
- [13] H. Behi *et al.*, "Thermal management analysis using heat pipe in the high current discharging of lithium-ion battery in electric vehicles," *Journal of Energy Storage*, vol. 32, p. 101893, 2020/12/01/ 2020, doi: <https://doi.org/10.1016/j.est.2020.101893>.
- [14] Y. F. Fung, M. F. Ercan, T. K. Ho, and W. L. Cheung, "Performance optimization for parallel processing on a multiple-CPU server," *Computer Physics Communications*, vol. 142, no. 1, pp. 191-195, 2001/12/15/ 2001, doi: [https://doi.org/10.1016/S0010-4655\(01\)00327-7](https://doi.org/10.1016/S0010-4655(01)00327-7).
- [15] J. Shen, J. Fang, H. Sips, and A. L. Varbanescu, "An application-centric evaluation of OpenCL on multi-core CPUs," *Parallel Computing*, vol. 39, no. 12, pp. 834-850, 2013/12/01/ 2013, doi: <https://doi.org/10.1016/j.parco.2013.08.009>.
- [16] R. J. McGlen, R. Jachuck, and S. Lin, "Integrated thermal management techniques for high power electronic devices," *Applied Thermal Engineering*, vol. 24, no. 8, pp. 1143-1156, 2004/06/01/ 2004, doi: <https://doi.org/10.1016/j.applthermaleng.2003.12.029>.
- [17] Y. Cai, Z. Li, J. Zhai, Y. Tang, and B. Yu, "Experimental investigation on a novel multi-branch heat pipe for multi-heat source electronics," *International Journal of Heat and Mass Transfer*, vol. 104, pp. 467-477, 2017/01/01/ 2017, doi: <https://doi.org/10.1016/j.ijheatmasstransfer.2016.08.080>.
- [18] J. H. Boo and H. G. Kim, "Experimental study on the performance characteristics of a cylindrical heat pipe having a screen wick subject to multiple heat sources," *Applied Thermal Engineering*, vol. 126, pp. 1209-1215, 2017/11/05/ 2017, doi: <https://doi.org/10.1016/j.applthermaleng.2017.02.097>.
- [19] N. Tharawadee, P. Terdtoon, and N. Kammuang-lue, "An investigation of thermal characteristics of a sintered-wick heat pipe with double heat sources," *American Journal of Applied Sciences*, vol. 10, pp. 1077-1086, 08/24 2013, doi: 10.3844/ajassp.2013.1077.1086.
- [20] L.-l. Jiang, Y. Tang, and M.-q. Pan, "Effects of bending on heat transfer performance of axial micro-grooved heat pipe," *Journal of Central South University*, vol. 18, no. 2, pp. 580-586, 2011/04/01 2011, doi: 10.1007/s11771-011-0734-2.
- [21] D. D. Odhekar and D. K. Harris, "Experimental investigation of bendable heat pipes using sintered copper felt wick," in *Thermal and Thermomechanical Proceedings 10th Intersociety Conference on Phenomena in Electronics Systems, 2006. ITherm 2006.*, 30 May-2 June 2006 2006, pp. 8 pp.-577, doi: 10.1109/ITHERM.2006.1645396.
- [22] L. Jiang, Y. Tang, and M.-q. Pan, "Effects of bending on heat transfer performance of axial micro-grooved heat pipe," *Journal of Central South University of Technology*, vol. 18, pp. 580-586, 04/01 2011, doi: 10.1007/s11771-011-0734-2.
- [23] J. P. Mooney, J. Punch, N. Jeffers, and V. Egan, "An accurate calorimeter-based method for the thermal characterization of heat pipes," *Experimental Thermal and Fluid Science*, p. 110381, 2021/02/25/ 2021, doi: <https://doi.org/10.1016/j.expthermflusci.2021.110381>.
- [24] A. Faghri and M. Buchko, "Experimental and Numerical Analysis of Low-Temperature Heat Pipes With Multiple Heat Sources," *Journal of Heat Transfer*, vol. 113, no. 3, pp. 728-734, 1991, doi: 10.1115/1.2910624.
- [25] S. J. Kline and F. A. McClintock, "Describing Uncertainties in Single-Sample Experiments (Am. Soc. Mech. Eng. 75, 3)," vol. 75, ed: Mechanical Engineering, 1953, pp. 3-8.
- [26] C. Liu, Q. Li, and D. Fan, "Fabrication and performance evaluation of flexible flat heat pipes for the thermal control of deployable structure," *International Journal of Heat and Mass Transfer*, vol. 144, p. 118661, 2019/12/01/ 2019, doi: <https://doi.org/10.1016/j.ijheatmasstransfer.2019.118661>.
- [27] H. Shabgard and A. Faghri, "Performance characteristics of cylindrical heat pipes with multiple heat sources," *Applied Thermal Engineering*, vol. 31, no. 16, pp. 3410-3419, 2011/11/01/ 2011, doi: <https://doi.org/10.1016/j.applthermaleng.2011.06.026>.
- [28] D. Deng, Y. Tang, G. Huang, L. Lu, and D. Yuan, "Characterization of capillary performance of composite wicks for two-phase heat transfer devices," *International Journal of Heat and Mass Transfer*, vol. 56, no. 1, pp. 283-293, 2013/01/01/ 2013, doi: <https://doi.org/10.1016/j.ijheatmasstransfer.2012.09.002>.
- [29] Y. Tang, D. Deng, L. Lu, M. Pan, and Q. Wang, "Experimental investigation on capillary force of composite wick structure by IR thermal imaging camera," *Experimental Thermal and Fluid Science*, vol. 34, no. 2, pp. 190-196, 2010/02/01/ 2010, doi: <https://doi.org/10.1016/j.expthermflusci.2009.10.016>.
- [30] A. Faghri and S. Thomas, "Performance Characteristics of a Concentric Annular Heat Pipe: Part I—Experimental Prediction and Analysis of the Capillary Limit," *Journal of Heat Transfer*, vol. 111, no. 4, pp. 844-850, 1989, doi: 10.1115/1.3250795.
- [31] S. Beyhaghi, S. Geoffroy, M. Prat, and K. M. Pillai, "Wicking and evaporation of liquids in porous wicks: A simple analytical approach to optimization of wick design," *AIChE Journal*, <https://doi.org/10.1002/aic.14353> vol. 60,

no. 5, pp. 1930-1940, 2014/05/01 2014, doi:
<https://doi.org/10.1002/aic.14353>.

- [32] J. P. Mooney, V. Egan, R. Quinlan, and J. Punch, "Effect of Multiple Heat Sources and Bend Angle on the Performance of Sintered Wicked Heat Pipes," in *2020 19th IEEE Intersociety Conference on Thermal and Thermomechanical Phenomena in Electronic Systems (ITherm)*, 21-23 July 2020 2020, pp. 124-133, doi: 10.1109/ITherm45881.2020.9190470.